Volume 48
Number 22
14 June 2024
Pages 9865–10326

NJC

New Journal of Chemistry

A journal for new directions in chemistry

rsc.li/njc

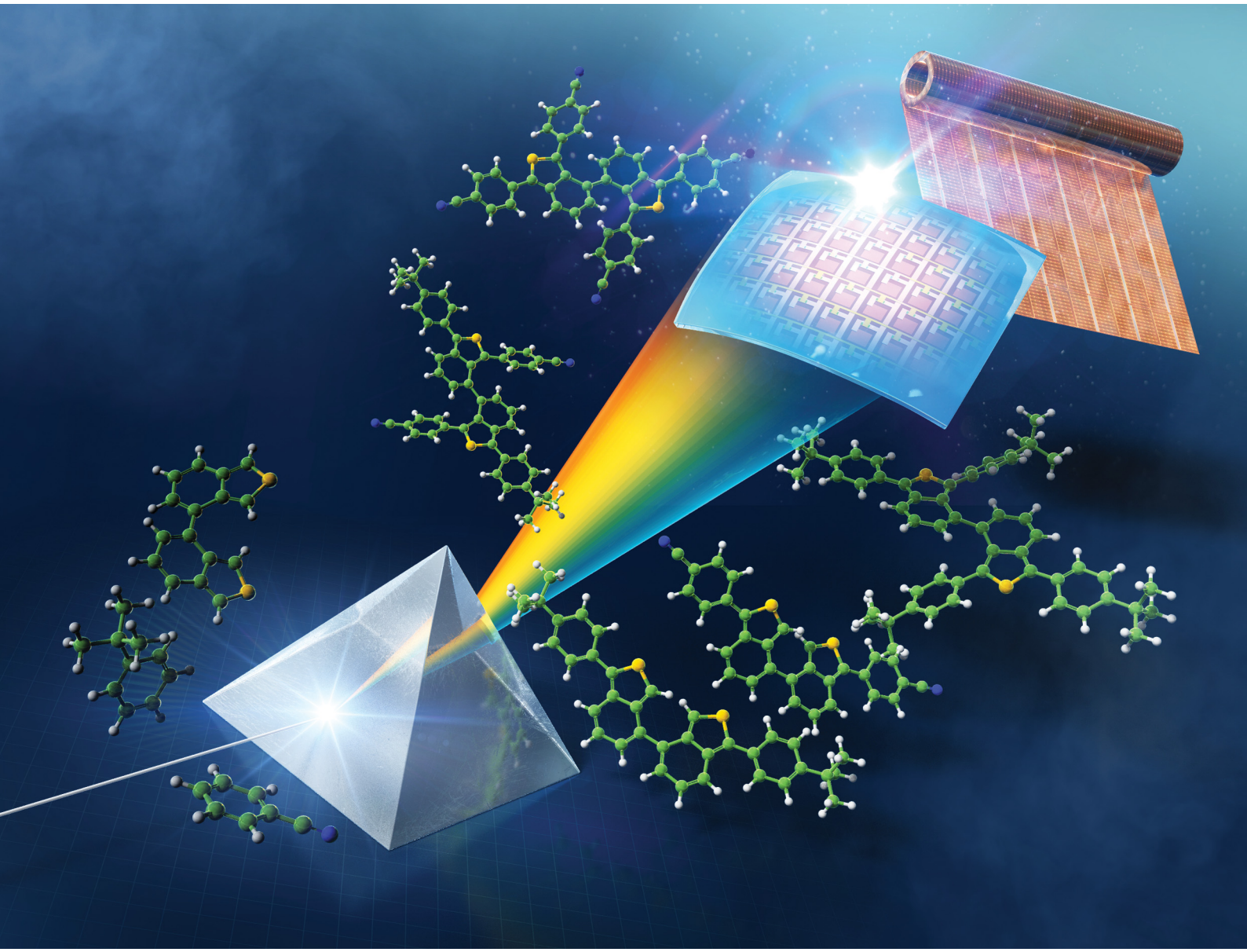

ISSN 1144-0546

ROYAL SOCIETY OF CHEMISTRY

PAPER

Yousuke Ooyama *et al.*

Synthesis, and optical and electrochemical properties of 1,1′,3,3′-tetraaryl-4,4′-bibenzo[*c*]thiophene derivatives with the same or different aryl substituents on the thiophene rings

cnrs

NJC

ROYAL SOCIETY OF CHEMISTRY

PAPER

View Article Online
View Journal | View Issue

Cite this: *New J. Chem.*, 2024, **48**, 9890

Synthesis, and optical and electrochemical properties of 1,1′,3,3′-tetraaryl-4,4′-bibenzo[*c*]thiophene derivatives with the same or different aryl substituents on the thiophene rings†

Yasuto Hara,[a] Kumpei Kozuka,[a] Keiichi Imato,[a] Seiji Akiyama,[b] Mio Ishida[b] and Yousuke Ooyama *[a]

We designed and synthesized 1,1′,3,3′-tetraaryl-4,4′-bibenzo[*c*]thiophene derivatives, 1,1′,3,3′-Ph*t*Bu-4,4′-BBT (**BBT-Ph*t*Bu4**), 1,1′,3,3′-PhCN-4,4′-BBT (**BBT-PhCN4**), and 1,1′-Ph*t*Bu-3,3′-PhCN-4,4′-BBT (**BBT-Ph*t*Bu2PhCN2**), which have four electron-donating *tert*-butylphenyl groups, four electron-withdrawing cyanophenyl groups, and two *tert*-butylphenyl groups and two cyanophenyl groups, respectively, on each thiophene ring by the Stille coupling reaction using 1,1′-diaryl-3,3′-distannyl-4,4′-BBT or 1,1′,3,3′-tetrastannyl-4,4′-BBT. It was found that the photoabsorption and fluorescence maximum wavelengths (λ_{max}^{abs} and λ_{max}^{fl}) of **BBT-Ph*t*Bu4**, **BBT-PhCN4**, and **BBT-Ph*t*Bu2PhCN2** appear in a longerwavelength region, in comparison with those of 1,1′-diaryl-4,4′-BBT derivatives **BBT-Ph*t*Bu2** with a *tert*-butylphenyl group and **BBT-PhCN2** with a cyanophenyl group on each thiophene ring. Moreover, the cyclic voltammetry (CV) curves of the 4,4′-BBT derivatives indicated that the introduction of the electron-donating *tert*-butylphenyl group and/or the electron-withdrawing cyanophenyl group into the benzo[*c*]thiophene skeleton leads to the lowering of the oxidation potential. In addition, an electron-donating phenyl substituent is more effective than an electron-withdrawing phenyl substituent in the lowering of the oxidation potential. Density functional theory (DFT) calculations as well as the experimental results revealed that increasing the number of electron-donating and electron-withdrawing phenyl groups on the thiophene ring results in the increase of the HOMO energy level and the lowering of the LUMO energy level, respectively, that leads to a decrease in the HOMO–LUMO band gap, that is, a bathochromic shift of the photoabsorption band. Thus, this work provides not only facile synthetic methods for 1,1′,3,3′-tetraaryl-4,4′-BBT derivatives with the same or different aryl substituents on the thiophene rings but also useful methods to precisely adjust their optical and electrochemical properties.

Received 22nd March 2024,
Accepted 29th April 2024

DOI: 10.1039/d4nj01350f

rsc.li/njc

Introduction

Benzo[*c*]thiophene and its derivatives have attracted significant attention as promising fluorophores for highly efficient bioimaging and phototheranostics[1] and key constituents of emitters, semiconductors and photosensitizers for organic optoelectronic devices such as organic field-effect transistors (OFETs),[2] organic photovoltaics (OPVs),[3] organic light-emitting diodes (OLEDs),[4] and dye-sensitized solar cells (DSSCs),[5] as well as scientific interest in synthetic organic chemistry, polymer chemistry, photochemistry, electrochemistry, and theoretical chemistry.[6] For this reason, some benzo[*c*]thiophene derivatives with substituents on the thiophene ring and/or the benzene ring, including 1,3- and 5,6-disubstituted benzo[*c*]thiophenes, have been synthesized, and their bioimaging, phototheranostic, and optoelectronic device performances as well as their photophysical and electrochemical properties were investigated so far.[1,7–9] Moreover, a few synthetic methods for 3,3′-disubstituted-1,1′-bibenzo[*c*]thiophenes as the 1,1′-dimer of benzo[*c*]thiophene have been developed by Cava,[10] Mohanakrishnan,[11] and Ono *et al.*[5] (Fig. 1a), although there are no reports on the synthesis of unsubstituted 1,1′-bibenzo[*c*]-thiophenes. In particular, the introduction of an aryl substituent with an electron-donating or electron-withdrawing group

[a] *Applied Chemistry Program, Graduate School of Advanced Science and Engineering, Hiroshima University, 1-4-1 Kagamiyama, Higashi-Hiroshima 739-8527, Japan. E-mail: yooyama@hiroshima-u.ac.jp*
[b] *Science & Innovation Center, Mitsubishi Chemical Corporation, 1000 Kamoshida-cho, Aoba-ku, Yokohama-shi, Kanagawa 227-8502, Japan*

† Electronic supplementary information (ESI) available. CCDC 2337948. For ESI and crystallographic data in CIF or other electronic format see DOI: **https://doi.org/10.1039/d4nj01350f**

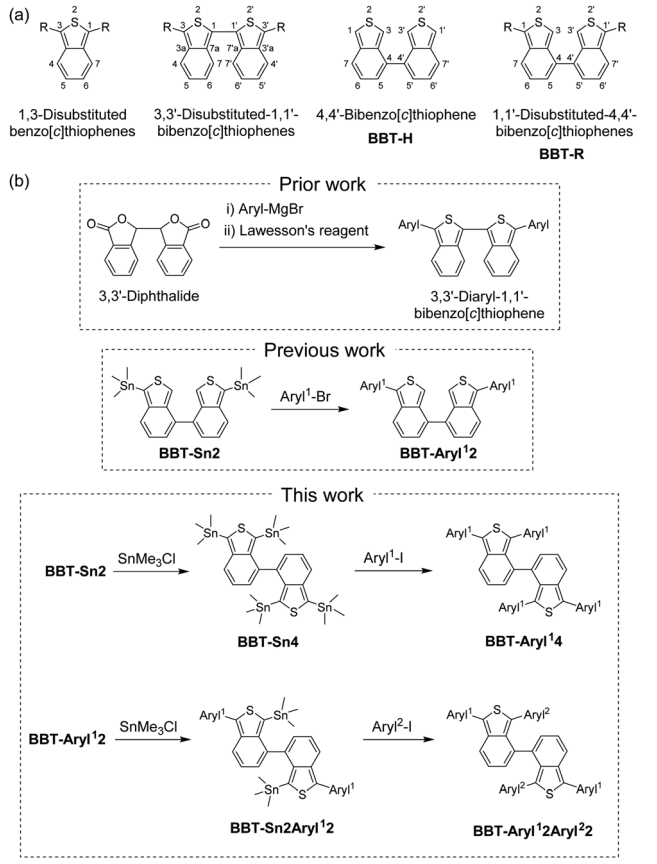

Fig. 1 (a) Chemical structures of benzo[*c*]thiophenes, 1,1′-bibenzo[*c*]-thiophenes, and 4,4′-bibenzo[*c*]thiophenes. (b) Prior work on 3,3′-diaryl-1,1′-bibenzo[*c*]thiophenes by Mohanakrishnan *et al.* (ref. 11), previous work (ref. 12) on 1,1′-diaryl-4,4′-bibenzo[*c*]thiophenes, and this work on 1,1′,3,3′-tetraaryl-4,4′-bibenzo[*c*]thiophenes.

on the benzo[*c*]thiophene chromophore allows us to adjust their optical and electrochemical properties due to the perturbation to the HOMO and the LUMO as well as the expansion of the π-conjugated system. Indeed, as a prior work for the synthetic methods, Mohanakrishnan *et al.* reported that 1,3-diarylbenzo[*c*]thiophenes and 3,3′-diaryl-1,1′-bibenzo[*c*]thiophenes have been prepared from 3-arylphthalide and diphthalide, respectively, *via* the lactone ring opening with an aryl Grignard reagent (ArMgBr) followed by thionation and concurrent intramolecular cyclization using Lawesson's reagent, and they revealed their optical and electrochemical properties (Fig. 1b).[9,11]

On the other hand, in our previous work, we offered new synthetic methods for 1,1′-diaryl-4,4′-bibenzo[*c*]thiophene (abbreviated as 1,1′-diaryl-4,4′-BBT), 1,1′-di-*tert*-butylphenyl-4,4′-BBT (**BBT-Ph*t*Bu2**) and 1,1′-dicyanophenyl-4,4′-BBT (**BBT-PhCN2**), using a Stille coupling reaction of 1,1′-distannyl-4,4′-BBT (**BBT-Sn2**) with an aryl halide and Suzuki coupling reaction of 1,1′-dibromo-4,4′-BBT (**BBT-Br2**) with arylboronic acid. Furthermore, we revealed their photophysical properties in the solution and the solid state, electrochemical properties, and X-ray crystal structures (Fig. 1b).[12] It was found that the bathochromic shift of the photoabsorption band from 4,4′-bibenzo[*c*]thiophene (**BBT-H**)[13] to **BBT-Ph*t*Bu2** and **BBT-PhCN2** is mainly attributed to the destabilization of the HOMO energy level for **BBT-Ph*t*Bu2** and both the destabilization of the HOMO energy level and the stabilization of the LUMO energy level for **BBT-PhCN2** due to the introduction of electron-donating *tert*-butylphenyl groups and the electron-withdrawing cyanophenyl groups, respectively, into the thiophene rings, leading to a decrease in the HOMO–LUMO band gap.

In this work, to further gain insight into not only the efficient synthetic route to aryl-substituted 4,4′-bibenzo[*c*]thiophene derivatives but also the effect of aryl substituents on the molecular structure and the photophysical and electrochemical properties, we designed 1,1′,3,3′-tetraaryl-4,4′-bibenzo[*c*]thiophene derivatives, 1,1′,3,3′-Ph*t*Bu-4,4′-BBT (**BBT-Ph*t*Bu4**), 1,1′,3,3′-PhCN-4,4′-BBT (**BBT-PhCN4**), and 1,1′-Ph*t*Bu-3,3′-PhCN-4,4′-BBT (**BBT-Ph*t*Bu2PhCN2**), which have four electron-donating *tert*-butylphenyl groups, four electron-withdrawing cyanophenyl groups, and two *tert*-butylphenyl groups and two cyanophenyl groups, respectively, on each thiophene ring (Fig. 1b). Herein, we provide facile synthetic methods for 1,1′,3,3′-tetraaryl-4,4′-bibenzo[*c*]thiophene derivatives with the same or different aryl substituents on the thiophene rings using the Stille coupling reaction employing 1,1′-diaryl-3,3′-distannyl-4,4′-BBT or 1,1′,3,3′-tetrastannyl-4,4′-BBT with an aryl halide and reveal their photophysical properties in the solution and the solid state, electrochemical properties, and X-ray crystal structures, in comparison with those of 1,1′-diaryl-4,4′-BBT derivatives.

Results and discussion

Synthesis

We found that **BBT-Sn2** is a useful intermediate to produce 1,1′,3,3′-tetraaryl-4,4′-BBT derivatives as well as 1,1′-diaryl-4,4′-BBT derivatives through the Stille coupling reaction with an aryl halide. In fact, our previous work demonstrated that **BBT-Ph*t*Bu2** and **BBT-PhCN2** are obtained in moderate yields (44% and 49%, respectively) using the Stille coupling reaction of 1,1′-distannyl-4,4′-BBT (**BBT-Sn2**) with the corresponding aryl halide (Scheme 1).[12] Moreover, for the preparation of 1,1′,3,3′-tetraaryl-4,4′-BBT derivatives with four same aryl substituents on the thiophene rings, 1,1′,3,3′-tetrastannyl-4,4′-BBT (**BBT-Sn4**) was derived from the reaction of **BBT-Sn2** with lithium diisopropylamide (LDA), followed by treatment with trimethyltin chloride. Thus, we conducted the Stille coupling reaction of **BBT-Sn4** with 1-*tert*-butyl-4-iodobenzene or 4-iodobenzonitrile using CuI and CsF in the presence of $Pd(PPh_3)_4$, because Baldwin *et al.* demonstrated that the combination of CuI and CsF can significantly promote the Stille reaction.[14] As a result, **BBT-Ph*t*Bu4** and **BBT-PhCN4** were successfully prepared, although the yields (17% and 25%) of the two tetraaryl-4,4′-BBT derivatives are lower than those of the corresponding diaryl-4,4′-BBT derivatives **BBT-Ph*t*Bu2** and **BBT-PhCN2** using Stille coupling reactions. The relatively low yields of **BBT-Ph*t*Bu4** and **BBT-PhCN4** are due to the production of the

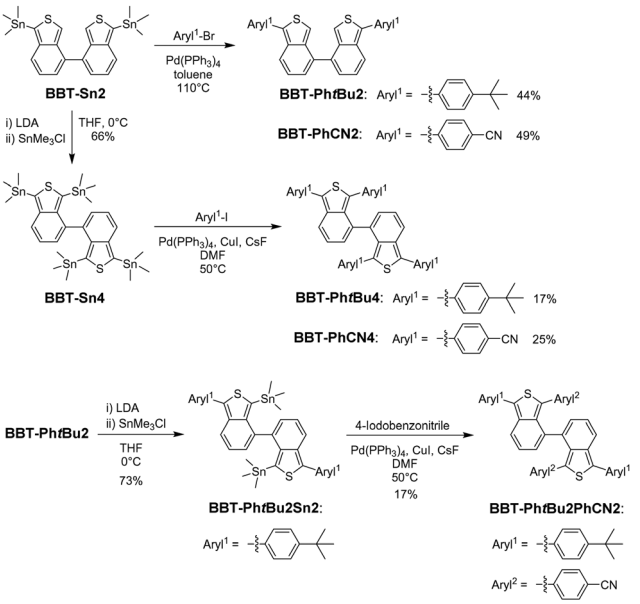

Scheme 1 Synthetic routes to 1,1′-diaryl-4,4′-bibenzo[*c*]thiophene derivatives **BBT-Ph*t*Bu2** and **BBT-PhCN2** (ref. 12) and 1,1′,3,3′-tetraaryl-4,4′-bibenzo[*c*]thiophene derivatives **BBT-Ph*t*Bu4**, **BBT-Ph*t*Bu2PhCN2**, and **BBT-PhCN4**.

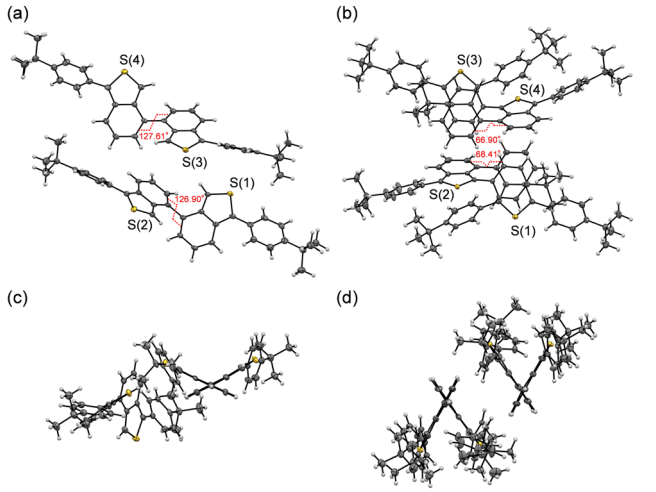

Fig. 2 Crystal structures from the (a) top view and (c) side view of **BBT-Ph*t*Bu2**, and the (b) top view and (d) side view of **BBT-Ph*t*Bu4**. The CH_2Cl_2 solvate in the crystal packing of **BBT-Ph*t*Bu4** was omitted to view more clearly the conformation of **BBT-Ph*t*Bu4**.

corresponding 1,1′,3-triaryl-4,4′-BBT derivative as well as the 1,1′-diaryl-4,4′-BBT derivatives **BBT-Ph*t*Bu2** or **BBT-PhCN2** as by-products. On the other hand, for the preparation of 1,1′,3,3′-tetraaryl-4,4′-BBT derivatives with two different aryl substituents on each thiophene ring, we prepared 1,1′-*tert*-butylphenyl-3,3′-distannyl-4,4′-BBT (**BBT-Sn2Ph*t*Bu2**) using the reaction of **BBT-Ph*t*Bu2** with LDA, followed by treatment with trimethyltin chloride. The Stille coupling of **BBT-Ph*t*Bu2Sn2** with 4-iodobenzonitrile gave **BBT-Ph*t*Bu2PhCN2** with a 4-cyanophenyl group and a *tert*-butylphenyl group on each thiophene ring with a yield of 17%. However, we could not produce 1,1′-PhCN-3,3′-Ph*t*Bu-4,4′-BBT (**BBT-PhCN2Ph*t*Bu2**) in the current stage because the dehydration of **BBT-PhCN2** by LDA, followed by di-stannylation did not proceed. Nevertheless, this result provides the stepwise synthetic method for the introduction of aryl substituents into the thiophene rings of the 4,4′-BBT skeleton, leading to the preparation of 1,1′,3,3′-tetraaryl-4,4′-BBT derivatives with the same or different aryl substituents on the thiophene rings.

X-ray crystal structures

In our previous work,[12] it was found that the crystal structure of **BBT-Ph*t*Bu2** has two crystallographically independent molecules in which the dihedral angles between the two benzo[*c*]thiophene units are 127.61 and 126.90°, respectively (Fig. 2a and c). For 1,1′,3,3′-tetraaryl-4,4′-BBT derivatives in this work, single-crystal X-ray structural analysis of **BBT-Ph*t*Bu4** was successfully made, while unfortunately we could not obtain single crystals of **BBT-PhCN4** and **BBT-Ph*t*Bu2PhCN2** with sufficient size to make the X-ray structural analysis possible. A single crystal of **BBT-Ph*t*Bu4** was grown from a mixed solvent of ethanol/dichloromethane. The obtained yellow plate crystal contained the CH_2Cl_2 solvate in the crystal packing (see the CIF file, ESI†). The crystal structure of **BBT-Ph*t*Bu4** has two crystallographically independent molecules, as with the crystal structure of **BBT-Ph*t*Bu2**, but in which the dihedral angles between the two benzo[*c*]thiophene units are 66.90 and 68.41°, respectively (Fig. 2b and d). This result shows that the two benzo[*c*]thiophene units in **BBT-Ph*t*Bu2** and **BBT-Ph*t*Bu4** have an *anti-clinal* (*ac*) and a *syn-clinal* (*sc*) conformation, respectively. Thus, 1,1′,3,3′-tetrasubstituted-4,4′-BBT derivatives seem to have a *sc* conformation because 1,1′,3,3′-tetrakis(*tert*-butyldimethylsilyl)-4,4′-BBT, which has been developed in our previous work, also forms a *sc* conformation in the crystal structure. On the other hand, the formation of one-dimensional continuous molecular chains by the intermolecular CH···S hydrogen bonding interactions[12] between the thiophene rings of neighboring molecules was observed in the crystal structure of **BBT-Ph*t*Bu2** (Fig. S16a, ESI†). Meanwhile, the short interatomic contacts between the carbon atom of the benzo[*c*]thiophene unit and the chlorine atom of CH_2Cl_2 were observed in the crystal structure of **BBT-Ph*t*Bu4** (Fig. S16b, ESI†). However, there are no short π–π contacts of less than 3.60 Å between the benzo[*c*]thiophene skeletons of the neighboring molecules of **BBT-Ph*t*Bu2** and **BBT-Ph*t*Bu4**, which indicates the absence of π–π interactions between the 4,4′-BBT fluorophores.

Optical properties in the solution and the solid state

The photoabsorption and fluorescence spectra of **BBT-H**, **BBT-Ph*t*Bu2**, **BBT-Ph*t*Bu4**, **BBT-Ph*t*Bu2PhCN2**, and **BBT-PhCN2** in toluene, and **BBT-PhCN4** in dichloromethane are shown in Fig. 3, and their photophysical data are summarized in Table 1. It was found that the 1,1′,3,3′-tetraaryl-4,4′-BBT as well as 1,1′-diaryl-4,4′-BBT show an intense photoabsorption maximum wavelength (λ_{max}^{abs} = 386–415 nm) with a relatively high molar extinction coefficient (ε_{max} = 20 600–27 000 M^{-1} cm^{-1}) in a longer wavelength region, in comparison with **BBT-H**

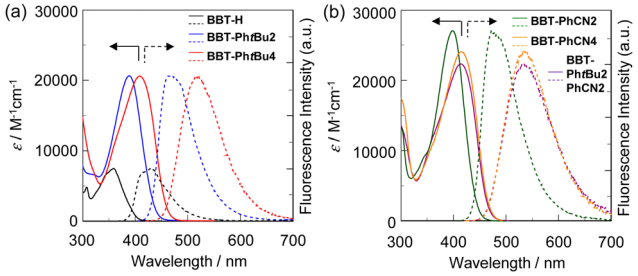

Fig. 3 (a) Photoabsorption (solid line) and fluorescence (dotted line) spectra ($\lambda^{ex} = \lambda^{abs}_{max}$) of **BBT-H**, **BBT-PhtBu2**, and **BBT-PhtBu4** (3.0 × 10^{-5} M) in toluene. (b) Photoabsorption (solid line) and fluorescence (dotted line) spectra ($\lambda^{ex} = \lambda^{abs}_{max}$) of **BBT-PhtBu2PhCN2** and **BBT-PhCN2** (*ca.* 3.0 × 10^{-5} M) in toluene, and **BBT-PhCN4** (3.0 × 10^{-5} M) in dichloromethane.

(λ^{abs}_{max} = 359 nm, ε_{max} = 7500 M^{-1} cm^{-1}). This result is due to the perturbation to the HOMO and the LUMO by the introduction of an aryl substituent with an electron-donating or electron-withdrawing group on the benzo[*c*]thiophene chromophore, as discussed later in density functional theory (DFT) and time-dependent DFT (TDDFT) calculations. Indeed, the λ^{abs}_{max} values of 1,1′,3,3′-tetraaryl-4,4′-BBT derivatives **BBT-PhtBu4** and **BBT-PhCN4** appear in a longer wavelength region by 23 nm and 16 nm, respectively, in comparison with those of 1,1′-diaryl-4,4′-BBT derivatives **BBT-PhtBu2** and **BBT-PhCN2**. Meanwhile, one can see that **BBT-PhCN2** and **BBT-PhCN4** with electron-withdrawing cyanophenyl groups exhibit λ^{abs}_{max} values in a longer wavelength region by 13 nm and 6 nm, respectively, in comparison with **BBT-PhtBu2** and **BBT-PhtBu4** with electron-donating *tert*-butylphenyl groups. Moreover, it was found that the λ^{abs}_{max} value of **BBT-PhtBu2PhCN2** with both cyanophenyl groups and *tert*-butylphenyl groups is the same as that of **BBT-PhCN4**, but appear in a longer wavelength region by 16 nm, compared to that of **BBT-PhtBu4**. As with the case of the photoabsorption band, the corresponding fluorescence maximum wavelengths (λ^{fl}_{max}) of the 4,4′-BBT derivatives appear in longer wavelength regions in the order of **BBT-H** (410 nm) < **BBT-PhtBu2** (469 nm) < **BBT-PhCN2** (472 nm) < **BBT-PhtBu4** (519 nm) < **BBT-PhCN4** (536 nm) ≈ **PhtBu2PhCN2** (537 nm). Meanwhile, the fluorescence quantum yield (Φ_{fl}) decreased in the order of **BBT-H** (0.41) > **BBT-PhtBu2** (0.39) > **BBT-PhtBu4** (0.28) ≈ **BBT-PhCN2** (0.27) > **BBT-PhCN4** (0.11) ≈ **PhtBu2PhCN2** (0.11).

Thus, in order to understand the difference in Φ_{fl} values between the 4,4′-BBT derivatives in the solutions, we performed time-resolved fluorescence spectroscopy. It was found that the fluorescence lifetimes (τ_{fl} = 1.27–1.88 ns) of **PhtBu2PhCN2**, **BBT-PhCN2**, and **BBT-PhCN4** are shorter than those (2.14–3.46 ns) of **BBT-H**, **BBT-PhtBu2**, and **BBT-PhtBu4**. The radiative rate constant (k_r = 2.13 × 10^8 s^{-1}) of **BBT-PhCN2** is somewhat larger than those (1.18–1.63 × 10^8 s^{-1}) of **BBT-H**, **BBT-PhtBu2**, and **BBT-PhtBu4**, meanwhile k_r values (5.85–8.21 × 10^7 s^{-1}) for **PhtBu2PhCN2** and **BBT-PhCN4** are about one-half those of **BBT-H** and **BBT-PhtBu2**. On the other hand, the nonradiative rate constants (k_{nr} = 4.73–6.64 × 10^8 s^{-1}) of **PhtBu2PhCN2**, **BBT-PhCN2**, and **BBT-PhCN4** are two to four times larger than those (1.70–3.36 × 10^8 s^{-1}) of **BBT-H**, **BBT-PhtBu2**, and **BBT-PhtBu4**. Consequently, the ratios of the nonradiative constant to the radiative constant (k_{nr}/k_r = 8.09, 2.70, and 8.09) of **PhtBu2PhCN2**, **BBT-PhCN2**, and **BBT-PhCN4** are larger than those (1.44, 1.56, and 2.56) of **BBT-H**, **BBT-PhtBu2**, and **BBT-PhtBu4**, indicating that the lower Φ_{fl} values of **PhtBu2PhCN2**, **BBT-PhCN2**, and **BBT-PhCN4** are mainly due to the larger k_{nr} value, compared to the Φ_{fl} values of **BBT-H**, **BBT-PhtBu2**, and **BBT-PhtBu4**. Therefore, this result provides a useful insight into the photophysical properties of 4,4′-BBT derivatives that increasing the number of phenyl substituents with electron-donating or electron-withdrawing groups on the thiophene ring leads to a bathochromic shift of λ^{abs}_{max} and λ^{fl}_{max} and lowering of the Φ_{fl} value. In addition, the increase in k_{nr} values of **PhtBu2PhCN2**, **BBT-PhCN2**, and **BBT-PhCN4** may be induced by rotation between electron-withdrawing cyanophenyl groups and the 4,4′-BBT fluorophore, leading to excited-state intramolecular charge transfer (ICT)-based fluorescence quenching.[15]

The solid-state photophysical properties of the as-recrystallized 4,4′-BBT derivatives have been investigated by solid-state UV-Vis diffuse reflection–photoabsorption and fluorescence spectral measurement (Fig. 4), and their photophysical data are summarized in Table 2. The photoabsorption spectrum of **BBT-PhtBu2** in the solid state shows a photoabsorption maximum wavelength ($\lambda^{abs\text{-}solid}_{max}$) at 400 nm which is similar to that in the solution. On the other hand, the photoabsorption bands of

Table 1 Photophysical and electrochemical data and HOMO and LUMO energy levels of 4,4′-bibenzo[*c*]thiophene derivatives in solution

Dye	λ^{abs}_{max}/nm (ε_{max}/M^{-1} cm^{-1})	λ^{fl}_{max}/nm (Φ_{fl})[c]	τ_{fl}[d]/ns	k_r[e]/s^{-1}	k_{nr}[f]/s^{-1}	k_{nr}/k_r	E^{ox}_{onset}[g]/V	E^{opt}_{g}[h]/eV	HOMO[i]/eV	LUMO[i]/eV
BBT-H[j]	359 (7500)[a]	410 (0.41)[a]	3.46[a]	1.18 × 10^{8} [a]	1.70 × 10^{8} [a]	1.44[a]	0.75[a]	3.16[a]	−5.55	−2.39
BBT-PhtBu2[j]	386 (20 700)[a]	469 (0.39)[a]	2.33[a]	1.68 × 10^{8} [a]	2.62 × 10^{8} [a]	1.56[a]	0.42[a]	2.87[a]	−5.22	−2.35
BBT-PhtBu4	409 (20 600)[a]	519 (0.28)[a]	2.14[a]	1.31 × 10^{8} [a]	3.36 × 10^{8} [a]	2.56[a]	0.26[a]	2.70[a]	−5.06	−2.36
BBT-PhtBu2PhCN2	415 (22 700)[a]	537 (0.11)[a]	1.34[a]	8.21 × 10^{7} [a]	6.64 × 10^{8} [a]	8.09[a]	0.54[a]	2.66[a]	−5.34	−2.68
BBT-PhCN2[j]	399 (27 000)[a]	472 (0.27)[a]	1.27[a]	2.13 × 10^{8} [a]	5.75 × 10^{8} [a]	2.70[a]	0.59[a]	2.82[a]	−5.39	−2.57
BBT-PhCN4	415 (24 100)[b]	536 (0.11)[b]	1.88[b]	5.85 × 10^{7} [b]	4.73 × 10^{8} [b]	8.09[b]	0.70[b]	2.65[b]	−5.50	−2.85

[a] In toluene. [b] In dichloromethane. [c] Fluorescence quantum yields (Φ_{fl}) were determined by using a calibrated integrating sphere system (λ^{ex} = 359 nm, 386 nm, 409 nm, 415 nm, 399 nm, and 415 nm for **BBT-H**, **BBT-PhtBu2**, **BBT-PhtBu4**, **BBT-PhtBu2PhCN2**, **BBT-PhCN2**, and **BBT-PhCN4**, respectively). [d] Fluorescence lifetime. [e] Radiative rate constant ($k_r = \Phi_{fl}/\tau_{fl}$). [f] Nonradiative rate constant ($k_{nr} = (1 - \Phi_{fl})/\tau_{fl}$). [g] Onset ($E^{ox}_{onset}$) *versus* Fc/Fc^+ of the oxidation potential. [h] Optical energy gaps (E^{opt}_{g}) were determined from the intersection (393 nm, 432 nm, 459 nm, 466 nm, 439 nm, and 468 nm for **BBT-H**, **BBT-PhtBu2**, **BBT-PhtBu4**, **BBT-PhtBu2PhCN2**, **BBT-PhCN2**, and **BBT-PhCN4**, respectively) of the photoabsorption and fluorescence spectra in toluene. [i] *Versus* vacuum level. [j] Previous work (ref. 12).

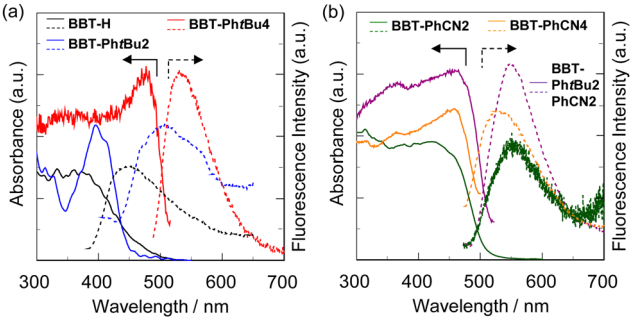

Fig. 4 Solid-state UV-vis diffuse reflection–absorption (solid line) and fluorescence (dotted line) spectra (λ^{ex} = 360 nm for **BBT-H** and **BBT-PhtBu2**, 477 nm for **BBT-PhtBu4**, 467 nm for **BBT-PhtBu2PhCN2**, 422 nm for **BBT-PhCN2**, and 459 nm for **BBT-PhCN4**) of (a) the as-recrystallized **BBT-H**, **BBT-PhtBu2**, **BBT-PhtBu4**, (b) **BBT-PhtBu2PhCN2**, **BBT-PhCN2**, and **BBT-PhCN4**.

BBT-H, **BBT-PhtBu4**, **PhtBu2PhCN2**, **BBT-PhCN2**, and **BBT-PhCN4** in the solid state are broadened in a longer wavelength region. In particular, the $\lambda_{max}^{abs\text{-}solid}$ values of **BBT-PhtBu4**, **PhtBu2PhCN2**, and **BBT-PhCN4** showed significant bathochromic shifts by 68 nm, 50 nm, and 44 nm, respectively, compared to those in the solution. Furthermore, the corresponding solid-state fluorescence spectra revealed that **BBT-H**, **BBT-PhtBu2**, **BBT-PhtBu4**, **BBT-PhtBu2PhCN2**, and **BBT-PhCN2** except **BBT-PhCN4** show a fluorescence maximum wavelength ($\lambda_{max}^{fl\text{-}solid}$) in a longer wavelength region by 45 nm, 41 nm, 12 nm, 10 nm, and 76 nm, respectively, compared to those in solution. The $\Phi_{fl\text{-}solid}$ values of **BBT-H**, **BBT-PhtBu4**, **PhtBu2PhCN2**, **BBT-PhCN2**, and **BBT-PhCN4** in the solid state are <0.02, 0.04, 0.09, 0.04, <0.02, and <0.02, respectively, which are significantly lower than those in solution (Table 1). Thus, the precise evaluations of the $\tau_{fl\text{-}solid}$ values for the 4,4′-BBT derivatives were difficult due to their feeble solid-state fluorescence properties. Consequently, for these 4,4′-BBT derivatives, the bathochromic shifts of λ_{max}^{abs} and λ_{max}^{fl} and the lowering of the Φ_{fl} value by changing from the solution to the solid state could be attributed to the formation of intermolecular π–π interactions between the 4,4′-BBT fluorophores, although it was not observed in the crystal structures of **BBT-PhtBu2** and **BBT-PhtBu4**, continuous intermolecular CH···S hydrogen bonding interactions between the fluorophores for **BBT-PhtBu2**, and/or the short interatomic contacts between the 4,4′-BBT fluorophore and CH_2Cl_2 solvate for **BBT-PhtBu4** in the solid state and consequent delocalization of excitons or excimers.[16]

Table 2 Photophysical data of 4,4′-bibenzo[c]thiophene derivatives in the solid state

Dye	$\lambda_{max}^{abs\text{-}solid}$/nm	$\lambda_{max}^{fl\text{-}solid}$/nm ($\Phi_{fl\text{-}solid}$)[a]
BBT-H[b]	360	455 (<0.02)
BBT-PhtBu2[b]	400	510 (0.04)
BBT-PhtBu4	477	531 (0.09)
BBT-PhtBu2PhCN2	465	547 (0.04)
BBT-PhCN2[b]	422	548 (<0.02)
BBT-PhCN4	459	527 (<0.02)

[a] Fluorescence quantum yields ($\Phi_{fl\text{-}solid}$) were determined by using a calibrated integrating sphere system (λ^{ex} = 360 nm for **BBT-H** and **BBT-PhtBu2**, 477 nm for **BBT-PhtBu4**, 467 nm for **BBT-PhtBu2PhCN2**, 422 nm for **BBT-PhCN2**, and 459 nm for **BBT-PhCN4**). [b] Previous work (ref. 12).

Electrochemical properties

The electrochemical properties of **BBT-H**, **BBT-PhtBu2**, **BBT-PhtBu4**, **BBT-PhtBu2PhCN2**, **BBT-PhCN2**, and **BBT-PhCN4** were investigated using cyclic voltammetry (CV) in acetonitrile, dichloromethane or DMF containing 0.1 M tetrabutylammonium perchlorate (Bu_4NClO_4). The potentials were internally referenced to ferrocene/ferrocenium (Fc/Fc^+). The cyclic voltammograms of the 4,4′-BBT derivatives are shown in Fig. 5, and their electrochemical data and the estimated HOMO and LUMO energy levels are summarized in Table 1. The cyclic voltammograms of the 4,4′-BBT derivatives showed an irreversible oxidation wave at 0.88 V for **BBT-H**, 0.55 V for **BBT-PhtBu2**, 0.52 V for **BBT-PhtBu4**, 0.76 V for **BBT-PhtBu2PhCN2**, 0.73 V for **BBT-PhCN2**, and 0.83 V for **BBT-PhCN4**, while any obvious reduction wave did not appear within the potential window (−1.5 to 0 V *versus* Fc/Fc^+). Thus, the oxidation waves of **BBT-PhtBu2**, **BBT-PhtBu4**, **BBT-PhtBu2PhCN2**, **BBT-PhCN2**, and **BBT-PhCN4** are cathodically shifted by 0.33 V, 0.36 V, 0.12 V, 0.15 V, and 0.05 V, respectively, compared to that of **BBT-H**. Indeed, this result indicates that the introduction of the electron-donating *tert*-butylphenyl group and/or the electron-withdrawing cyanophenyl group into the thiophene ring leads to the lowering of the oxidation potential. In addition, an electron-donating phenyl substituent is more effective than an electron-withdrawing phenyl substituent in the lowering of the oxidation potential.

The HOMO energy levels ($-[E_{onset}^{ox} + 4.8]$ eV) *versus* vacuum level were estimated from the onset potentials (E_{onset}^{ox}) of the oxidation waves, and the LUMO energy levels were estimated from the E_{onset}^{ox} and the intersections (optical energy gap: E_g^{opt}) of the photoabsorption and fluorescence spectra in solution (Table 1). The HOMO energy levels rise in the order of **BBT-H** (−5.55 eV) < **BBT-PhCN4** (−5.50 eV) < **BBT-PhCN2** (−5.39 eV) < **BBT-PhtBu2PhCN2** (−5.34 eV) < **BBT-PhtBu2** (−5.22 eV) < **BBT-PhtBu4** (−5.06 eV), so that the HOMO energy levels of

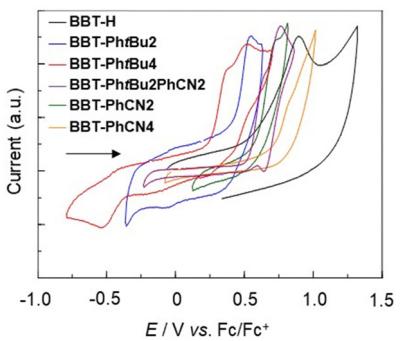

Fig. 5 Cyclic voltammograms of **BBT-H** and **BBT-PhtBu2** in acetonitrile containing 0.1 M Bu_4NClO_4, **BBT-PhtBu2** and **BBT-PhtBu2PhCN2** in dichloromethane containing 0.1 M Bu_4NClO_4, and **BBT-PhCN2** and **BBT-PhCN4** in DMF containing 0.1 M Bu_4NClO_4 at a scan rate of 100 mV s^{-1}. The arrow denotes the direction of the potential scan.

BBT-Ph*t*Bu2 and **BBT-Ph*t*Bu4** are significantly higher than those of the other 4,4′-BBT derivatives. On the other hand, the LUMO energy levels lower in the order of **BBT-Ph*t*Bu2** (−2.35 eV) ≈ **BBT-Ph*t*Bu4** (−2.36 eV) > **BBT-H** (−2.39 eV) > **BBT-PhCN2** (−2.57 eV) > **BBT-Ph*t*Bu2PhCN2** (−2.68 eV) > **BBT-PhCN4** (−2.85 eV). Thus, this result indicates that the LUMO energy levels of **BBT-Ph*t*Bu2PhCN2**, **BBT-PhCN2**, and **BBT-PhCN4** are much lower than those of **BBT-H**, **BBT-Ph*t*Bu2**, and **BBT-Ph*t*Bu4**, although the LUMO energy levels of **BBT-H**, **BBT-Ph*t*Bu2**, and **BBT-Ph*t*Bu4** are similar to each other. The fact reveals that the bathochromic shift of the photoabsorption band from **BBT-H** to **BBT-Ph*t*Bu2** and **BBT-Ph*t*Bu4** is mainly attributed to the destabilization of the HOMO energy level through the introduction of electron-donating *tert*-butylphenyl groups into the benzo[*c*]thiophene skeleton, leading to a decrease in the HOMO–LUMO band gap. In contrast, the HOMO and LUMO energy levels of **BBT-Ph*t*Bu2PhCN2**, **BBT-PhCN2**, and **BBT-PhCN4** are somewhat higher and significantly lower, respectively, than those of **BBT-H**. Consequently, the bathochromic shift of the photoabsorption band from **BBT-H** to **BBT-Ph*t*Bu2PhCN2**, **BBT-PhCN2**, and **BBT-PhCN4** is mainly attributed to the stabilization of the LUMO energy level through the introduction of the electron-withdrawing cyanophenyl group into the benzo[*c*]thiophene skeleton, resulting in a decrease in the HOMO–LUMO band gap. Therefore, it was found that increasing the number of electron-donating or electron-withdrawing phenyl groups on the thiophene ring results in the increase of the HOMO energy level or the lowering of the LUMO energy level, respectively, so this result provides a useful method to precisely adjust the HOMO and LUMO energy levels of 4,4′-BBT derivatives.

Theoretical calculations

The electronic structures and molecular orbitals of **BBT-H**, **BBT-Ph*t*Bu2**, **BBT-Ph*t*Bu4**, **BBT-Ph*t*Bu2PhCN2**, **BBT-PhCN2**, and **BBT-PhCN4** were derived from DFT calculations at the B3LYP/6-31G(d,p) level[17] (Fig. 6). The DFT calculations demonstrated that the HOMO of **BBT-H** is delocalized on each benzo[*c*]-thiophene unit, but the HOMOs of the other 4,4′-BBT derivatives are mainly delocalized on each benzo[*c*]thiophene unit, although the HOMOs of two benzo[*c*]thiophenes are practically independent because the HOMO−1 energy level is very close to the HOMO energy level (Fig. S18, ESI†). The LUMOs of **BBT-H**, **BBT-Ph*t*Bu2**, and **BBT-Ph*t*Bu4** are mainly delocalized over the whole benzo[*c*]thiophene skeletons through 4,4′-positions. On the other hand, it is worth mentioning here that the LUMOs of **BBT-Ph*t*Bu2PhCN2**, **BBT-PhCN2**, and **BBT-PhCN4** are delocalized over the whole benzo[*c*]thiophene skeletons containing the cyanophenyl groups through 4,4′-positions. It was found that the HOMO energy levels of **BBT-Ph*t*Bu2** and **BBT-Ph*t*Bu4** are higher than that of **BBT-H**, but their LUMO energy levels are similar to each other. The HOMO and LUMO energy levels of **BBT-PhCN2** and **BBT-PhCN4** are significantly lower than those of **BBT-H**, but the lowering of the LUMO energy levels is larger than that of the HOMO energy levels, although the CV showed that the HOMO energy levels of **BBT-PhCN2** and **BBT-PhCN4** are higher than that of **BBT-H**. Meanwhile, the HOMO energy level of **BBT-Ph*t*Bu2PhCN2** is nearly equal to that of **BBT-H**, but its LUMO energy level is much lower than that of **BBT-H**. Consequently, the HOMO–LUMO band gaps decrease in the order of **BBT-H** (3.74 eV) > **BBT-Ph*t*Bu2** (3.56 eV) > **BBT-PhCN2** (3.32 eV) > **BBT-Ph*t*Bu4** (3.19 eV) > **BBT-Ph*t*Bu2PhCN2** (3.12 eV) ≈ **BBT-PhCN4** (3.10 eV). Thus, the DFT calculation suggested that compared to **BBT-H**, the increase of the HOMO energy level for **BBT-Ph*t*Bu2** and **BBT-Ph*t*Bu4** and the lowering of the LUMO energy level for **BBT-Ph*t*Bu2PhCN2**, **BBT-PhCN2**, and **BBT-PhCN4** result in a decrease in the HOMO–LUMO band gap from **BBT-H** to the 1,1′-diaryl-4,4′-BBT and 1,1′,3,3′-tetraaryl-4,4′-BBT derivatives, as in the case of experimental results.

Furthermore, the TDDFT calculations were performed to elucidate the photophysical properties of the 4,4′-BBT derivatives

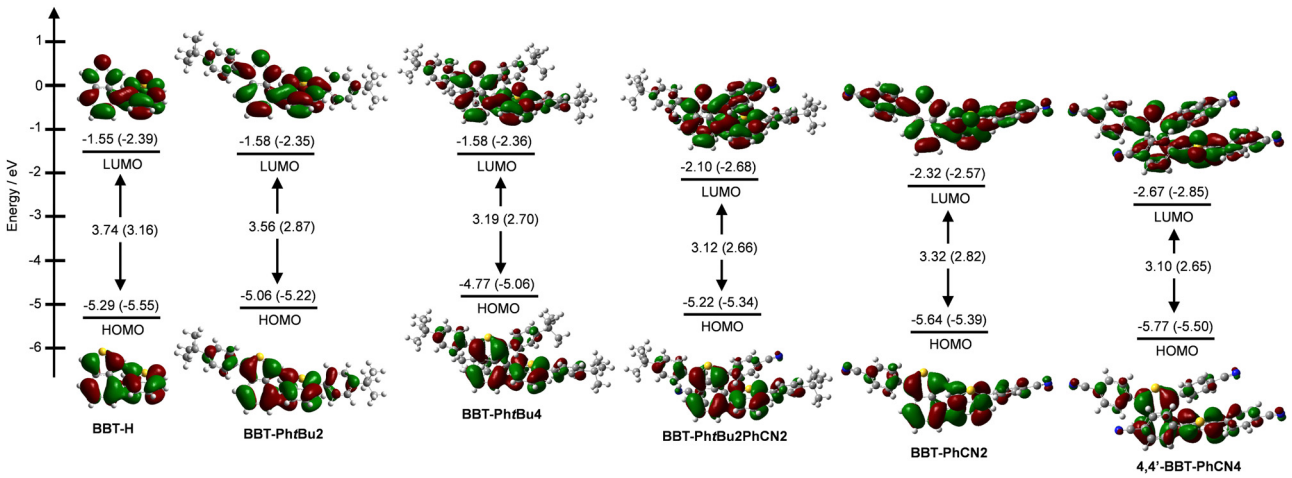

Fig. 6 Energy level diagram, HOMO and LUMO of **BBT-H**, **BBT-Ph*t*Bu2**, **BBT-Ph*t*Bu2**, **BBT-Ph*t*Bu2PhCN2**, **BBT-PhCN2**, and **BBT-PhCN4** derived from DFT calculations at the B3LYP/6-31G(d,p) level. For all the 4,4′-BBT derivatives the optimized geometries are a *syn-clinal* (*sc*) conformation. Numbers in parentheses are the experimental values (Table 1).

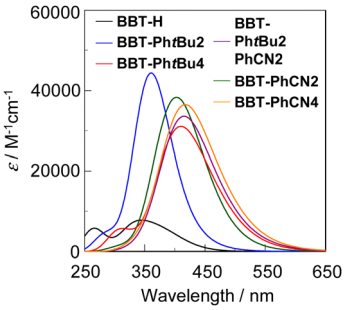

Fig. 7 Photoabsorption spectra of **BBT-H**, **BBT-PhtBu2**, **BBT-PhtBu2**, **BBT-PhtBu2PhCN2**, **BBT-PhCN2**, and **BBT-PhCN4** derived from TD-DFT calculations.

(Fig. 7). The calculated $\lambda_{max}^{abs\text{-}calcd}$ and ε_{calcd} values of the 4,4′-BBT derivatives are 345 nm and 7800 M^{-1} cm^{-1} for **BBT-H**, 361 nm and 44 300 M^{-1} cm^{-1} for **BBT-PhtBu2**, 410 nm and 31 100 M^{-1} cm^{-1} for **BBT-PhtBu4**, 416 nm and 33 600 M^{-1} cm^{-1} for **BBT-PhtBu2PhCN2**, 403 nm and 38 300 M^{-1} cm^{-1} for **BBT-PhCN2**, and 417 nm and 36 500 M^{-1} cm^{-1} for **BBT-PhCN2**. The $S_0 \rightarrow S_1$ transitions are mainly attributed to the transitions from the HOMO to the LUMO (67% for **BBT-H**, 88% for **BBT-PhtBu2**, 93% for **BBT-PhtBu4**, 88% for **BBT-PhtBu2PhCN2**, 93% for **BBT-PhCN2**, and 90% for **BBT-PhCN4**). Indeed, the TD-DFT calculations are in good agreement with the experimental results of the bathochromic shift of the photoabsorption band from **BBT-H** to **BBT-PhtBu2**, **BBT-PhCN2**, **BBT-PhtBu4**, **BBT-PhtBu2PhCN4**, and **BBT-PhCN4**, although there are differences in the ε_{calcd} values between the experimental and TD-DFT calculation results.

Experimental

General

Melting points were measured with an AS ONE ATM-02. IR spectra were recorded using a SHIMADZU IRTracer-100 by the ATR method. ^{1}H NMR spectra were recorded using a Varian-400 FT NMR spectrometer. High-resolution mass spectral data by APCI was acquired using a Thermo Fisher Scientific LTQ Orbitrap XL. Recycling gel permeation chromatography (GPC) was performed using an RI-detector (SHIMADZU RID-20A), a UV-detector (SHIMADZU SPD-20A), and a pump (SHIMADZU LC-20A) with two columns (Shodex GPC FP-2002). Photoabsorption spectra of solutions were recorded with a Shimadzu UV-3600 plus spectrophotometer. Photoabsorption spectra of solids were recorded using a Shimadzu UV-3600 plus spectrophotometer with a calibrated integrating sphere system. Fluorescence spectra of solutions and solids were recorded with a HORIBA FluoroMax-4 spectrofluorometer. The fluorescence quantum yields in solution and in the solid state were determined using a HORIBA FluoroMax-4 spectrofluorometer with a calibrated integrating sphere system. Fluorescence decay measurements were performed with a HORIBA DeltaFlex modular fluorescence lifetime system, using a Nano-LED pulsed diode excitation source (370 nm). Cyclic voltammetry (CV) curves were recorded in an acetonitrile/Bu_4NClO_4 (0.1 M), dichloromethane/Bu_4NClO_4 (0.1 M), or DMF/Bu_4NClO_4 (0.1 M) solution with a three-electrode system consisting of Ag/Ag^+ ($AgNO_3$ in acetonitrile/Bu_4NClO_4, dichloromethane/Bu_4NClO_4, or DMF/Bu_4NClO_4) as the reference electrode, a Pt plate as the working electrode and Pt wire as the counter electrode using an Electrochemical Measurement System HZ-7000 (HOKUTO DENKO).

Synthesis

1,1′,3,3′-Tetra(trimethylstannyl)-4,4′-bibenzo[*c*]thiophene (BBT-Sn4). To a THF solution (0.43 ml) of **BBT-Sn2** (0.10 g, 0.17 mmol) under a nitrogen atmosphere at 0 °C was added dropwise a 1.0 M hexane/THF solution of lithium diisopropylamide (1.0 ml, 1.0 mmol). After stirring for 3.5 h, a 1.0 M hexane solution of trimethyltin chloride (1.0 ml, 1.0 mmol) was added dropwise. The reaction mixture was further stirred for 19 h at room temperature. The reaction mixture was quenched with water, and then, the solution was extracted with ethyl acetate. The ethyl acetate extract was dried over anhydrous $MgSO_4$, filtered and concentrated to give **BBT-Sn4** (0.10 g, yield 66%) as a brown solid; m.p. 188–189 °C; FT-IR (ATR): $\tilde{\nu}$ = 2959, 2918, 2853, 1508, 1470 cm^{-1}; ^{1}H NMR (400 MHz, acetone-d_6): δ = −0.21 (s, 18H), 0.54 (s, 18H), 7.36 (d, J = 5.4 Hz, 2H), 7.58 (dd, J = 6.4 and 8.7 Hz, 2H), 8.18 (d, J = 7.6 Hz, 2H) ppm; HRMS (APCI): m/z (%): [M + H^+] calcd for $C_{28}H_{42}S_2Sn_4$, 922.88886; found 922.89098.

1,1′,3,3′-Tetra(4-(*tert*-buthyl)phenyl)-4,4′-bibenzo[*c*]thiophene (BBT-PhtBu4). A solution of **BBT-Sn4** (0.16 g, 0.17 mmol), 1-*tert*-butyl-4-iodobenzene (0.30 ml, 1.7 mmol), CsF (0.15 g, 1.0 mmol), CuI (0.0065 g, 0.034 mmol), and $Pd(PPh_3)_4$ (0.020 g, 0.017 mmol) in DMF (35 ml) was stirred for 20 h at 50 °C under a nitrogen atmosphere. After vacuum filtration of the reaction mixture, the solution was extracted with dichloromethane. The dichloromethane extract was dried over anhydrous $MgSO_4$, filtered and concentrated. Recycling GPC ($CHCl_3$ as the eluent) for the residue was performed to give **BBT-PhtBu4** (0.024 g, yield 17%) as a yellow solid; m.p. 230–231 °C; FT-IR (ATR): $\tilde{\nu}$ = 2959, 2901, 2866, 1520, 1458, 1362, 1267 cm^{-1}; ^{1}H NMR (400 MHz, acetone-d_6): δ = 0.98 (s, 18H), 1.39 (s, 18H), 6.75 (d, J = 8.1 Hz, 4H), 6.80 (d, J = 8.7 Hz, 4H), 7.10 (dd, J = 6.5 and 8.9 Hz, 2H), 7.19 (d, J = 5.5 Hz, 2H), 7.49 (d, J = 8.9 Hz, 2H), 7.52 (d, J = 8.7 Hz, 4H), 7.56 (d, J = 8.7 Hz, 4H) ppm; it was difficult to obtain the ^{13}C NMR spectrum due to the low solubility of **BBT-PhtBu4** in any deuterated solvents; HRMS (APCI): m/z (%): [M + H^+] calcd for $C_{56}H_{58}S_2$, 795.40527; found 795.40717.

1,1′,3,3′-Tetra(4-cyanophenyl)-4,4′-bibenzo[*c*]thiophene (BBT-PhCN4). A solution of **BBT-Sn4** (0.18 g, 0.19 mmol), 4-iodobenzonitrile (0.44 g, 1.9 mmol), CsF (0.17 g, 1.1 mmol), CuI (0.0072 g, 0.038 mmol), and $Pd(PPh_3)_4$ (0.022 g, 0.019 mmol) in DMF (40 ml) was stirred for 20 h at 50 °C under a nitrogen atmosphere. After vacuum filtration of the reaction mixture, the solution was extracted with dichloromethane. The dichloromethane extract was dried over anhydrous $MgSO_4$, filtered and concentrated. The residue was chromatographed on silica gel (dichloromethane : hexane = 3 : 1 as the eluent) to give **BBT-PhCN4** (0.033 g, yield 25%) as a yellow solid; m.p. 300 °C or more; FT-IR (ATR): $\tilde{\nu}$ = 2922, 2222, 1599, 1510 cm^{-1}; ^{1}H NMR (400 MHz, CD_2Cl_2): δ = 6.88 (d, J = 7.8 Hz, 4H), 7.06 (d, J = 8.5 Hz,

4H), 7.27 (dd, J = 6.6 and 8.9 Hz, 2H), 7.40 (d, J = 5.8 Hz, 2H), 7.59 (d, J = 8.9 Hz, 2H), 7.65 (d, J = 8.5 Hz, 4H), 7.83 (d, J = 8.6 Hz, 4H) ppm; it was difficult to obtain the ^{13}C NMR spectrum due to the low solubility of **BBT-PhCN4** in any deuterated solvents; HRMS (APCI): m/z (%): [M^+] calcd for $C_{44}H_{22}N_4S_2$, 670.12804; found 670.12933.

1,1′-Bis(4-(*tert*-butyl)phenyl)-[4,4′-bibenzo[*c*]thiophene]-3,3′-bis(trimethylstannyl) (BBT-Ph*t*Bu2Sn2). To a THF solution (0.49 ml) of **BBT-Ph*t*Bu2** (0.12 g, 0.22 mmol) under a nitrogen atmosphere at 0 °C was added dropwise a 1.0 M hexane/THF solution of lithium diisopropylamide (1.3 ml, 1.3 mmol). After stirring for 3.5 h, a 1.0 M hexane solution of trimethyltin chloride (1.3 ml, 1.3 mmol) was added dropwise. The reaction mixture was further stirred for 15 h at room temperature. The reaction mixture was quenched with water, and then, the solution was extracted with ethyl acetate. The ethyl acetate extract was dried over anhydrous $MgSO_4$, filtered, and concentrated to give **BBT-Ph*t*Bu2Sn2** (0.14 g, yield 73%) as a brown solid; m.p. 197–198 °C; FT-IR (ATR): $\tilde{\nu}$ = 2961, 2866, 1605, 1508, 1458, 1395, 1362 cm^{-1}; ^{1}H NMR (400 MHz, acetone-d_6): δ = −0.10 (s, 18H), 1.41 (s, 18H), 7.07 (d, J = 6.4 Hz, 2H), 7.27 (dd, J = 6.4 and 8.8 Hz, 2H), 7.64 (d, J = 8.7 Hz, 4H), 7.68 (d, J = 8.6 Hz, 4H), 7.98 (d, J = 8.9 Hz, 2H) ppm; HRMS (APCI): m/z (%): [M + H^+] calcd for $C_{42}H_{50}S_2Sn_2$, 859.14706; found 859.14829.

1,1′-Bis(4-(*tert*-butyl)phenyl)-[4,4′-bibenzo[*c*]thiophene]-3,3′-bis(4-cyanophenyl) (BBT-Ph*t*Bu2PhCN2). A solution of **BBT-Ph*t*Bu2Sn2** (0.081 g, 0.095 mmol), 4-iodobenzonitrile (0.11 g, 0.48 mmol), CsF (0.044 g, 0.29 mmol), CuI (0.0036 g, 0.019 mmol), and $Pd(PPh_3)_4$ (0.011 g, 0.0095 mmol) in DMF (35 ml) was stirred for 23 h at 50 °C under a nitrogen atmosphere. After vacuum filtration of the reaction mixture, the solution was extracted with dichloromethane. The dichloromethane extract was dried over anhydrous $MgSO_4$, filtered and concentrated. The residue was chromatographed on silica gel (dichloromethane : hexane = 1 : 1 as the eluent) to give **BBT-Ph*t*Bu2PhCN2** (0.012 g, yield 17%) as a yellow solid; m.p. 300 °C or more; FT-IR (ATR): $\tilde{\nu}$ = 2961, 2866, 2224, 1601, 1460, 1364 cm^{-1}; ^{1}H NMR (400 MHz, CD_2Cl_2): δ = 1.40 (s, 18H), 6.87 (d, J = 8.0 Hz, 4H), 7.06 (d, J = 8.5 Hz, 4H), 7.16 (dd, J = 6.6 and 8.9 Hz, 2H), 7.34 (d, J = 6.4 Hz, 2H), 7.45 (d, J = 8.3 Hz, 4H), 7.55–7.58 (m, 6H) ppm; it was difficult to obtain the ^{13}C NMR spectrum due to the low solubility of **BBT-Ph*t*Bu2PhCN2** in any deuterated solvents; HRMS (APCI): m/z (%): [M + H^+] calcd for $C_{50}H_{40}N_2S_2$, 733.27057; found 733.27228.

X-ray crystallographic analysis

The reflection data of **BBT-Ph*t*Bu4** were collected at 100 K on a Rigaku XtaLAB Synergy-R/DW diffractometer using monochromated Mo-Kα (λ = 0.71073 Å). The structure was solved by the SHELXT 2014/5 method and refined based on full-matrix least squares on F^2 using SHELXL-2018/3. The non-hydrogen atoms were refined anisotropically. Hydrogen atoms were fixed geometrically and not refined. Crystallographic data have been deposited in the Cambridge Crystallographic Data Centre (CCDC 2337948†).

Crystal of BBT-Ph*t*Bu4. A single crystal of **BBT-Ph*t*Bu4** was recrystallized from a mixed solvent of ethanol/dichloromethane as a yellow plate crystal, and was air stable. Crystallographic data: $C_{57}H_{60}Cl_2S_2$, M = 880.07, triclinic, a = 14.4868(3), b = 15.5221(5), c = 22.5994(6) Å, α = 75.521(2)°, β = 80.754(2)°, γ = 84.376(2)°, V = 4847.6(2) Å^3, D_{calcd} = 1.206 g cm^{-3}, space group $P\bar{1}$ (no. 2), Z = 4, 22 621 reflections measured, 23 124 unique (R_{int} = 0.0521), which were used in all calculations. The final R_1(reflections) = 0.0623 (16 714) [$I > 2\sigma(I)$], wR_2(reflections) = 0.1634 (23 124). GOF = 1.015.

Conclusions

We developed 1,1′,3,3′-tetraaryl-4,4′-bibenzo[*c*]thiophene derivatives, **BBT-Ph*t*Bu4** with four electron-donating *tert*-butylphenyl groups, **BBT-PhCN4** with four electron-withdrawing cyanophenyl groups, and **BBT-Ph*t*Bu2PhCN2** with two *tert*-butylphenyl groups and two cyanophenyl groups on each thiophene ring using the Stille coupling reaction with 1,1′-diaryl-3,3′-distannyl-4,4′-BBT or 1,1′,3,3′-tetrastannyl-4,4′-BBT and revealed their photophysical and electrochemical properties and X-ray crystal structures, in comparison with those of 1,1′-diaryl-4,4′-BBT derivatives **BBT-Ph*t*Bu2** with a *tert*-butylphenyl group and **BBT-PhCN2** with a cyanophenyl group on each thiophene ring. It was found that increasing the number of phenyl substituents with electron-donating or electron-withdrawing groups on the thiophene ring led to not only the bathochromic shift of λ^{abs}_{max} and λ^{fl}_{max} but also the lowering of the Φ_{fl} value. The DFT calculations, as well as the cyclic voltammetry and photophysical analyses, revealed that increasing the number of electron-donating and electron-withdrawing phenyl groups on the thiophene ring results in the increase of the HOMO energy level and the lowering of the LUMO energy level, respectively, which leads to a decrease in the HOMO–LUMO band gap, that is, a bathochromic shift of the photoabsorption band. This finding offers a useful method to precisely adjust the HOMO and LUMO energy levels of 4,4′-BBT derivatives. Therefore, this work provides not only facile synthetic methods for 1,1′,3,3′-tetraaryl-4,4′-bibenzo[*c*]thiophene derivatives with the same or different aryl substituents on the thiophene rings but also useful methods to precisely adjust their optical and electrochemical properties. Further studies on the development of donor–π–acceptor (D–π–A)-type 1,1′,3,3′-tetraaryl-4,4′-BBT derivatives exhibiting intermolecular charge transfer (ICT) characteristics are now in progress to gain insight into the effects of electron-donating and electron-withdrawing aryl substituents on the optical and electrochemical properties of 4,4′-BBT derivatives.

Conflicts of interest

There are no conflicts to declare.

Acknowledgements

This work was supported by Grants-in-Aid for Scientific Research (B) from the Japan Society for the Promotion of Science (JSPS) KAKENHI Grant Number 22H02123.

Notes and references

1 (*a*) Y. Tan, Y. Sun, W. Huang, D. Zhu, D. Yan, D. Wang and B. Z. Tang, *Luminescence*, 2024, **39**, e4606; (*b*) K.-W. Lee, Y. Cao, W.-C. Wei, J.-H. Tan, Y. Wan, Z. Feng, Y. Zhang, Y. Liu, X. Zheng, C. Cao, H. Chen, P. Wang, S. Li, K.-T. Wong and C.-S. Lee, *Adv. Mater.*, 2023, **35**, 2211632; (*c*) D. Yan, M. Wang, Q. Wu, N. Niu, M. Li, R. Song, J. Rao, M. Kang, Z. Zhang, F. Zhou, D. Wang and B. Z. Tang, *Angew. Chem., Int. Ed.*, 2022, **61**, e202202614; (*d*) D. Yan, W. Xie, J. Zhang, L. Wang, D. Wang and B. Z. Tang, *Angew. Chem., Int. Ed.*, 2021, **60**, 26769–26776.

2 (*a*) X. Chen, D. Zhang, Y. He, M. U. Ali, Y. Wu, C. Zhao, P. Wu, C. Yan, F. Wudl and H. Meng, *Mater. Chem. Front.*, 2020, **4**, 3578–3584; (*b*) K. Yamamoto, Y. Ie, M. Nitani, N. Tohnai, F. Kakiuchi, K. Zhang, W. Pisula, K. Asadi, P. W. M. Blom and Y. Aso, *J. Mater. Chem. C*, 2018, **6**, 7493–7500; (*c*) C. P. Yu, R. Kimura, T. Kurosawa, E. Fukuzaki, T. Watanabe, H. Ishii, S. Kumagai, M. Yano, J. Takeya and T. Okamoto, *Org. Lett.*, 2019, **21**, 4448–4453.

3 (*a*) Y. Qin, J. Y. Kim, C. D. Frisbie and M. A. Hillmyer, *Macromolecules*, 2008, **41**, 5563–5570; (*b*) M. R. Raj and S. Anandan, *RSC Adv.*, 2013, **3**, 14595–14608; (*c*) J. D. Douglas, G. Griffini, T. W. Holcombe, E. P. Young, O. P. Lee, M. S. Chen and J. M. J. Fréchet, *Macromolecules*, 2012, **45**, 4069–4074.

4 Y.-C. Hu, Z.-L. Lin, T.-C. Huang, J.-W. Lee, W.-C. Wei, T.-Y. Ko, C.-Y. Lo, D.-G. Chen, P.-T. Chou, W.-Y. Hung and K.-T. Wong, *Mater. Chem. Front.*, 2020, **4**, 2029–2039.

5 (*a*) Q. Liu, F.-T. Kong, T. Okujima, H. Yamada, S.-Y. Dai, H. Uno, N. Ono, X.-Z. You and Z. Shen, *Tetrahedron Lett.*, 2012, **53**, 3264–3267; (*b*) Q. Liu, Q.-Y. Feng, H. Yamada, Z.-S. Wang, N. Ono, X.-Z. You and Z. Shen, *Chem. – Asian J.*, 2012, **7**, 1312–1319.

6 (*a*) F. Wudl, M. Kobayashi and A. J. Heeger, *J. Org. Chem.*, 1984, **49**, 3382–3384; (*b*) H. Meng and F. Wudl, *Macromolecules*, 2001, **34**, 1810–1816; (*c*) O. D. Abrbanel, J. Rozon and G. R. Hutchison, *J. Phys. Chem. Lett.*, 2022, **13**, 2158–2164; (*d*) G. Grover, J. D. Tovar and M. Kertesz, *J. Phys. Chem. C*, 2022, **126**, 5302–5310; (*e*) G. Grover, G. M. Peters, J. D. Tovar and M. Kertesz, *Phys. Chem. Chem. Phys.*, 2020, **22**, 11431–11439.

7 (*a*) S. T. Meek, E. E. Nesterov and T. M. Swager, *Org. Lett.*, 2008, **10**, 2991–2993; (*b*) K. Kawabata and H. Goto, *J. Mater. Chem.*, 2012, **22**, 23514–23524; (*c*) U. Mitschke and P. Bäuerle, *J. Chem. Soc., Perkin Trans. 1*, 2001, 740–753; (*d*) T. V. Hughes and M. P. Cava, *J. Org. Chem.*, 1999, **64**, 313–315.

8 (*a*) M. Hori, T. Kataoka, H. Shimizu, J. Hongo and M. Kido, *J. Chem. Soc., Perkin Trans. 1*, 1989, 1611–1618; (*b*) R. H. L. Kiebooms, P. J. A. Adriaensens, D. J. M. Vanderzande and J. M. J. V. Gelan, *J. Org. Chem.*, 1997, **62**, 1473–1480; (*c*) J. W. Terpstra and A. M. van Leusen, *J. Org. Chem.*, 1986, **51**, 230–238; (*d*) R. M. El-Shishtawy, K. Fukunishi and S. Miki, *Tetrahedron Lett.*, 1995, **36**, 3177–3180.

9 (*a*) A. K. Mohanakrishnan and P. Amaladass, *Tetrahedron Lett.*, 2005, **46**, 4225–4229; (*b*) A. K. Mohanakrishnan, N. S. Kumar and P. Amaladass, *Tetrahedron Lett.*, 2008, **49**, 4792–4795; (*c*) J. A. Clement, P. Gunasekaran and A. K. Mohanakrishnan, *Tetrahedron*, 2009, **65**, 4113–4123; (*d*) N. S. Kumar and A. K. Mohanakrishnan, *Tetrahedron*, 2010, **66**, 5660–5670; (*e*) G. G. Rajeshwaran, M. Nandakumar, R. Sureshbabu and A. K. Mohanakrishnan, *Org. Lett.*, 2011, **13**, 1270–1273.

10 (*a*) Y. Okuda, M. V. Lakshmikantham and M. P. Cava, *J. Org. Chem.*, 1991, **56**, 6024–6026; (*b*) E. Aqad, M. V. Lakshmikantham and M. P. Cava, *Org. Lett.*, 2004, **6**, 3039–3041.

11 (*a*) A. K. Mohanakrishnan, P. Amaladass and J. A. Clement, *Tetrahedron Lett.*, 2007, **48**, 779–784; (*b*) P. Amaladass, J. A. Clement and A. K. Mohanakrishnan, *Eur. J. Org. Chem.*, 2008, 3798–3810.

12 T. Higashino, Y. Hara, K. Imato, S. Akiyama, M. Ishida and Y. Ooyama, *New J. Chem.*, 2023, **47**, 9555–9559.

13 (*a*) K. Obayashi, T. Higashino, K. Imato and Y. Ooyama, *New J. Chem.*, 2021, **45**, 13258–13261; (*b*) K. Obayashi, K. Imato, S. Aoyama, T. Enoki, S. Akiyama, M. Ishida, S. Suga, K. Mitsudo and Y. Ooyama, *RSC Adv.*, 2021, **11**, 18870–18880; (*c*) K. Obayashi, S. Miho, M. Yasui, K. Imato, S. Akiyama, M. Ishida and Y. Ooyama, *New J. Chem.*, 2021, **45**, 17085–17094.

14 S. P. H. Mee, V. Lee and J. E. Baldwin, *Angew. Chem., Int. Ed.*, 2004, **43**, 1132–1136.

15 (*a*) D. Liese and G. Haberhauer, *Isr. J. Chem.*, 2018, **58**, 813–826; (*b*) C. Yan, Z. Guo, W. Chi, W. Fu, S. A. A. Abedi, X. Liu, H. Tian and W.-H. Zhu, *Nat. Commun.*, 2021, **12**, 3869.

16 (*a*) H. Langhals, T. Potrawa, H. Nöth and G. Linti, *Angew. Chem., Int. Ed. Engl.*, 1989, **28**, 478–480; (*b*) H.-C. Yeh, W.-C. Wu, Y.-S. Wen, D.-C. Dai, J.-K. Wang and C.-T. Chen, *J. Org. Chem.*, 2004, **69**, 6455–6462; (*c*) Y. Ooyama, T. Nakamura and K. Yoshida, *New J. Chem.*, 2005, **29**, 447–456.

17 M. J. Frisch, G. W. Trucks, H. B. Schlegel, G. E. Scuseria, M. A. Robb, J. R. Cheeseman, G. Scalmani, V. Barone, G. A. Petersson, H. Nakatsuji, X. Li, M. Caricato, A. V. Marenich, J. Bloino, B. G. Janesko, R. Gomperts, B. Mennucci, H. P. Hratchian, J. V. Ortiz, A. F. Izmaylov, J. L. Sonnenberg, D. Williams-Young, F. Ding, F. Lipparini, F. Egidi, J. Goings, B. Peng, A. Petrone, T. Henderson, D. Ranasinghe, V. G. Zakrzewski, J. Gao, N. Rega, G. Zheng, W. Liang, M. Hada, M. Ehara, K. Toyota, R. Fukuda, J. Hasegawa, M. Ishida, T. Nakajima, Y. Honda, O. Kitao, H. Nakai, T. Vreven, K. Throssell, J. A. Montgomery, Jr., J. E. Peralta, F. Ogliaro, M. J. Bearpark, J. J. Heyd, E. N. Brothers, K. N. Kudin, V. N. Staroverov, T. A. Keith, R. Kobayashi, J. Normand, K. Raghavachari, A. P. Rendell, J. C. Burant, S. S. Iyengar, J. Tomasi, M. Cossi, J. M. Millam, M. Klene, C. Adamo, R. Cammi, J. W. Ochterski, R. L. Martin, K. Morokuma, O. Farkas, J. B. Foresman and D. J. Fox, *Gaussian 16, Revision B.01 and C.01*, Gaussian, Inc., Wallingford CT, 2016.

